Experimental validation of connected automated vehicle design among human-driven vehicles

Jin I. Ge[a,b], Sergei S. Avedisov[a], Chaozhe R. He[a], Wubing B. Qin[a], Mehdi Sadeghpour[a], Gábor Orosz[a,*]

[a] *Department of Mechanical Engineering, University of Michigan, Ann Arbor, MI 48109, USA*
[b] *Department of Computing and Mathematical Sciences, California Institute of Technology, Pasadena, CA 91125, USA*

ARTICLE INFO

ABSTRACT

In this paper, we present results regarding the experimental validation of connected automated vehicle design. In order for a connected automated vehicle to integrate well with human-dominated traffic, we propose a class of connected cruise control algorithms with feedback structure originated from human driving behavior. We test the connected cruise controllers using real vehicles under several driving scenarios while utilizing beyond-line-of-sight motion information obtained from neighboring human-driven vehicles via vehicle-to-everything (V2X) communication. We experimentally show that the design is robust against variations in human behavior as well as changes in the topology of the communication network. We demonstrate that both safety and energy efficiency can be significantly improved for the connected automated vehicle as well as for the neighboring human-driven vehicles and that the connected automated vehicle may bring additional societal benefits by mitigating traffic waves.

1. Introduction

The advances in automotive and infrastructure technologies have revolutionized the safety and efficiency of road transportation in the past few decades. While traffic accidents and congestion problems continue to exist on our roadways (NTSHA, 2016; Schrank et al., 2015), advancements in automated driving technologies promise a much safer and highly efficient future of transportation (Stern et al., 2018; Aeberhard et al., 2015; Mersky and Samaras, 2016). However, many automated vehicles today only use on-board sensors to perceive the environment, which may not be robust to various driving conditions. In particular, as on-board sensors are only able to obtain current information about the immediate neighborhood (Harding et al., 2014), these automated vehicles often have difficulties anticipating the motion of surrounding vehicles reliably. Therefore, many disengagement incidents happen when an automated vehicle has to interact with nearby human-driven vehicles (California DMV, 2016).

In order to facilitate the implementation of automated vehicles in real traffic, it is desirable to introduce beyond-line-of-sight information through vehicle-to-vehicle (V2V) or vehicle-to-infrastructure (V2I) communication (Montemerlo et al., 2015; Urmson et al., 2017). These are often grouped as vehicle-to-everything (V2X) where X may also incorporate other traffic participants like pedestrians or bicyclists. Previous studies have found that V2X communication may further amplify the benefits of driving automation (Vander Werf et al., 2002; Shladover et al., 2015; Talebpour and Mahmassani, 2016). A prominent application of V2X communication is cooperative adaptive cruise control (CACC) where a group of automated vehicles follow each other while

---

* Corresponding author at: Department of Mechanical Engineering, University of Michigan, Ann Arbor, MI 48109, USA.
  E-mail addresses: jge@caltech.edu (J.I. Ge), avediska@umich.edu (S.S. Avedisov), hchaozhe@umich.edu (C.R. He), wubing@umich.edu (W.B. Qin),
mehsad@umich.edu (M. Sadeghpour), orosz@umich.edu (G. Orosz).

coordinating their motion via V2X communication (van Arem et al., 2006; Shladover, 2007; Milanes et al., 2011; Shladover et al., 2012; Wang et al., 2014a,b; Ploeg et al., 2014b; Zheng et al., 2017; Li et al., 2017). In particular, CACC has the potential to improve fuel economy and traffic throughput (di Bernardo et al., 2015; Milanes and Shladover, 2014; Zhou et al., 2017; Lioris et al., 2017). However, as the penetration rate of automated vehicles is low, it is rare to find several of them driving consecutively on road, which may severely limit the implementation of CACC in real traffic (Shladover et al., 2015).

Thus, it is desirable to consider connected automated vehicle design in partially automated traffic environments (Jiang et al., 2017; Luo et al., 2016). In particular, we proposed connected cruise control (CCC) that is able to utilize motion information from multiple human-driven vehicles ahead (Orosz, 2016; Ge et al., 2017). Despite being categorized as an advanced form of CACC (Shladover et al., 2015), CCC exhibits different challenges from most CACC implementations. For example, CACC implementations often assume a priori knowledge about the parameters of each vehicle in the platoon (van Nunen et al., 2012; Englund et al., 2016), while CCC needs to be robust against variations is human parameters (Ge and Orosz, 2016). Furthermore, while most CACC research assume fixed communication topology among vehicles (Ploeg et al., 2014a; Turri et al., 2017), CCC allows the connected automated vehicle to select which motion signals are incorporated into its controller based on ad hoc V2X communication (Zhang and Orosz, 2016; Ge and Orosz, 2014; Qin and Orosz, 2017). Such flexibility allows ad hoc connected vehicle systems to form consisting of connected automated vehicles and surrounding human-driven vehicles equipped with V2X devices. When designed appropriately, the connected automated vehicle may reduce velocity fluctuations significantly and thus improve the safety, fuel economy and lead to smooth traffic flow of human-dominated traffic systems (He and Orosz, 2017; Avedisov and Orosz, 2017; He et al., 2018).

However, in order to harvest the aforementioned theoretical benefits, connected cruise control needs to be validated in real-world scenarios. Experimental and simulation studies on CACC have brought into life the benefits of exchanging motion information among automated vehicles (van Nunen et al., 2012; Mersky and Samaras, 2016; Sepulcre et al., 2013). Yet it remains a question whether motion information from real human-driven vehicles can indeed benefit a connected automated vehicle. As human car-following behaviors are much more volatile than automated driving systems, such experimental validations are indispensable for connected cruise control (Orosz et al., 2017). Therefore, in this paper, we conduct experiments both on a closed track and on public roads to examine the benefits of utilizing motion information from human-driven vehicles ahead for a connected automated vehicle.

By using real vehicles we experimentally validate that the connected cruise control design can be robust against changes in the car-following behaviors of preceding vehicles and the topology of the V2X communication network. That is, a connected cruise controller can handle the rich behavior of real human drivers ahead; and it can still be used when some of the surrounding human-driven vehicles are not broadcasting. We also demonstrate through experiments on public roads that appropriately designed CCC algorithms can mitigate traffic waves traveling along chains of human-driven vehicles, and thus, improve the safety and energy efficiency of the connected automated vehicle as well as the neighboring human-driven vehicles. That is, for the first time, we demonstrate that a single connected automated vehicle, which utilizes beyond-line-of-sight information appropriately, may improve human-dominated traffic flow while being integral part of the flow. These results validate the feasibility of CCC implementation in real-world scenarios and the experiments also suggest future research directions in connected automated vehicle design.

The rest of this paper is organized as follows: in Section 2 we describe the human car-following behavior that can be used as a base for the design of the longitudinal control of connected automated vehicles; in Section 3 we design a class of longitudinal controllers for the connected automated vehicle used in the experiments; in Section 4 we describe the experimental setup and the functionalities; in Section 5 we present a set of experiments that demonstrate how a connected automated vehicle can improve safety using motion information from multiple preceding vehicles; in Section 6 we present a set of experiments demonstrating traffic wave mitigation and improvements of energy efficiency; finally in Section 7 we conclude our results and discuss future directions.

2. Human car-following model

In this section, we model the car-following behavior of human drivers, which will later be serve as a base for the control design of the connected automated vehicle. For simplicity, we consider two vehicles driving consecutively in a single lane; see Fig. 1(a).

Based on (Orosz, 2016; Ge et al., 2017), we describe the dynamics of the human-driven vehicle i as
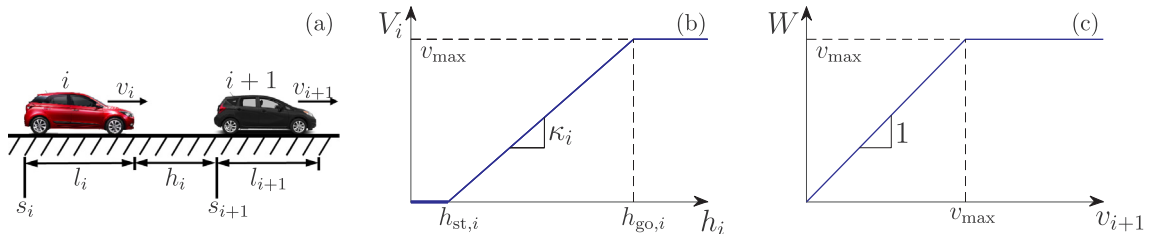

Fig. 1. (a) Single-lane car-following of human-driven vehicles showing the positions s_i, s_{i+1}, the velocities v_i, v_{i+1}, and the distance headway $h_i = s_{i+1} - s_i - l_i$. (b) The range policy (3) where v_{max} is the speed limit, $h_{st,i}$ is the smallest distance headway before the vehicle intends to stop, and $h_{go,i}$ is the largest headway after which the vehicle intends to maintain v_{max}. The gradient κ_i is also highlighted in the figure. (c) The function (4) used for avoiding car-following when the predecessor is speeding.

$$\dot{s}_i(t) = v_i(t),$$
$$\dot{v}_i(t) = \alpha_{\text{h},i}(V_i(h_i(t-\tau_i)) - v_i(t-\tau_i)) + \beta_{\text{h},i}(W(v_{i+1}(t-\tau_i)) - v_i(t-\tau_i)). \tag{1}$$

Here the dot stands for differentiation with respect to time t, s_i denotes the position of the rear bumper of vehicle i while v_i denotes its speed. Moreover, h_i denotes the distance headway, that is, that bumper-to-bumper distance between vehicle i and its predecessor:

$$h_i = s_{i+1} - s_i - l_i, \tag{2}$$

where l_i is the length of vehicle i, as shown in Fig. 1(a).

According to (1) the acceleration is determined by two terms: the difference between the headway-dependent desired velocity and the actual velocity, and the velocity difference between the vehicle and its predecessor. The gains $\alpha_{\text{h},i}$ and $\beta_{\text{h},i}$ are used to correct velocity errors, while the delay τ_i represents the sum of driver reaction time and actuator delay of the vehicle. The desired velocity is determined by the nonlinear range policy function

$$V_i(h_i) = \begin{cases} 0 & \text{if} \quad h_i \leqslant h_{\text{st},i}, \\ \kappa_i(h_i - h_{\text{st},i}) & \text{if} \quad h_{\text{st},i} < h_i < h_{\text{go},i}, \\ v_{\max} & \text{if} \quad h_i \geqslant h_{\text{go},i}, \end{cases} \tag{3}$$

shown in Fig. 1(b), where $\kappa_i = v_{\max}/(h_{\text{go},i} - h_{\text{st},i})$. That is, the desired velocity is zero for small distances ($h_i \leq h_{\text{st},i}$) and equal to the speed limit $v_{\max}$ for large distances ($h_i \geq h_{\text{go},i}$). Between these, the desired velocity increases with the headway linearly, with gradient κ_i, whose inverse is often called the time headway.

In (1), the saturation function

$$W(v_{i+1}) = \begin{cases} v_{i+1} & \text{if} \quad v_{i+1} \leqslant v_{\max}, \\ v_{\max} & \text{if} \quad v_{i+1} > v_{\max}, \end{cases} \tag{4}$$

shown in Fig. 1(c) is included to handle the situation when a human-driven vehicle refuses to go beyond the speed limit $v_{\max}$ while its predecessor is speeding.

For $v_i(t) < v_{\max}$, (3) defines the steady-state behavior of vehicle i and, in aggregation, the steady-state traffic flow where vehicles travel with the same constant velocity:

$$s_i(t) = v^* t + \bar{s}_i, \qquad v_i(t) \equiv v^*, \tag{5}$$

such that

$$\bar{s}_{i+1} - \bar{s}_i - l_i = h_i^*, \qquad v^* = V_i(h_i^*). \tag{6}$$

In a vehicle string, the equilibrium velocity v^* is determined by the head vehicle while the equilibrium distance h_i^* can be calculated from the range policy (3). While the model (1, 3,4) does not include the limits of engine/brakes and the physical effects such as rolling resistance, air drag, and road grades, this simple model is able to capture the human car-following behavior and allow parameter identification using experimental data (Ge and Orosz, 2017). Similar models have been used to discuss how the longitudinal dynamics of individual vehicles may influence the traffic flow in aggregation (Orosz et al., 2010; Wagner, 2010).

While the car-following model (1, 3,4) is widely used to study characteristics of human-dominated traffic flow, it cannot perfectly capture all features of volatile human car-following behaviors. As an example, Fig. 2 shows the motion of a pair of human-driven cars during one experiment where the curves are colored according to cars shown in Fig. 1. In Fig. 2(a), the preceding vehicle (black) performs two nearly identical braking maneuvers at around $t = 400$ [s] and $t = 440$ [s]. While the following vehicle (red) over-reacts and slows down to 10 [m/s] responding to the first maneuver, in the second maneuver it reacts mildly and only reaches 13.5 [m/s]. In contrast, with parameters $v_{\max} = 30$ [m/s], $h_{\text{st},i} = 5$ [m], $\kappa_i = 1$ [1/s], $\alpha_{\text{h},i} = 0.1$ [1/s], $\beta_{\text{h},i} = 0.5$ [1/s], $\tau_i = 1$ [s], the car-following model (1, 3,4) generates similar responses (dashed) when responding to both maneuvers, with minimum speed at around 10.5 [m/s]. Moreover, after $t = 450$ [s] the following vehicle experiences non-negligible speed variations despite little speed variations in the preceding vehicle, which the car-following model (1, 3,4) cannot reproduce. Indeed, differences between the modelled and actual human car-following behaviors can also be observed in the distance headway in Fig. 2(b).

To sum up, the model (1, 3,4) can capture the human car-following behavior qualitatively, and thus, it will be used as a base for the connected cruise control design in the next section. However, such models cannot fully describe the rich human car-following behavior seen in Fig. 2. Therefore, when incorporating motion information from multiple human-driven vehicles ahead, the connected cruise controller needs to be tested among real human-driven vehicles in order to prove its robustness against unmodeled variations of human behaviors.

3. Longitudinal controller design for the connected automated vehicle

In this section we present the longitudinal controller for the connected automated vehicle used in the experiments. In order to be easily implemented and readily accepted by the passengers and other road users, the longitudinal controller is designed to have similar feedback structure as in the human car-following model (1) and (3). We consider the scenario where a connected automated vehicle 0 (blue) receives motion information from several human-driven vehicles ahead; see Fig. 3(a). The blue arrows indicate that the connected cruise controller contains feedback terms using the motion information of the preceding vehicles.

We write the dynamics of this connected automated vehicle as
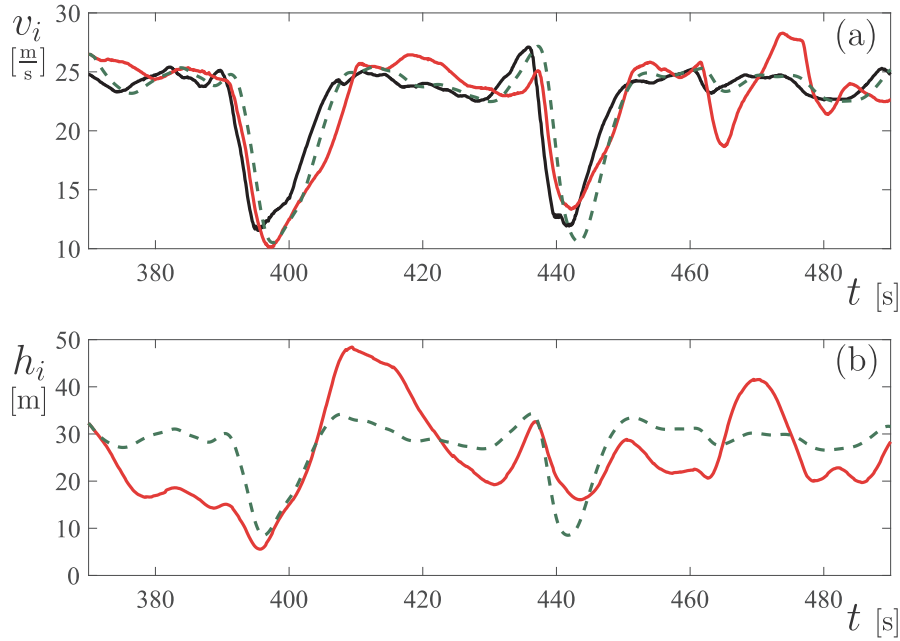
Fig. 2. Motion data for a pair of human-driven vehicles (solid curves) and corresponding simulated trajectories by the car-following model (1, 3,4) (dashes curves). (a) The speed data of the preceding vehicle (solid black) and the following vehicle (solid red), and the simulated speed of the following vehicle (dashed green). (b) The headway data (solid red) and simulated headway (dashed green) of the following vehicle. (For interpretation of the references to colour in this figure legend, the reader is referred to the web version of this article.)
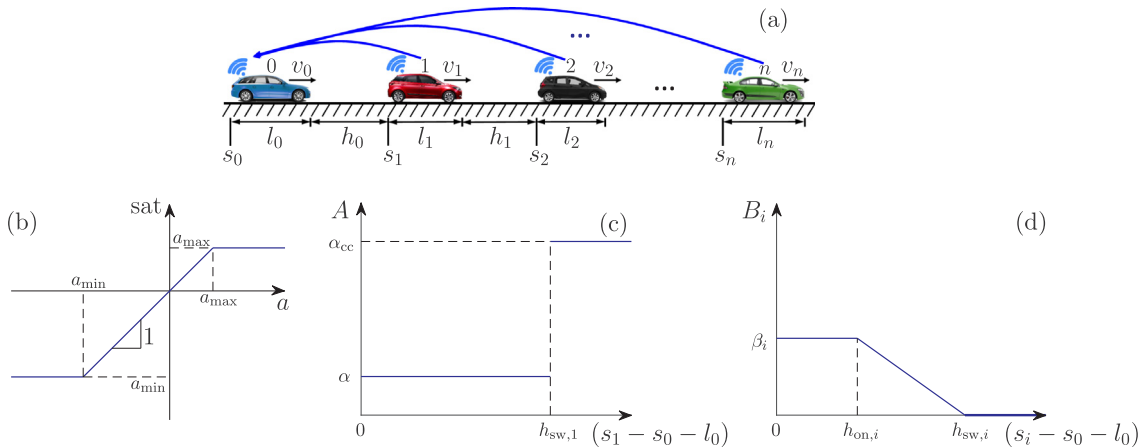
Fig. 3. (a) The connected vehicle system setup: a string of $n + 1$ vehicles on a single-lane road where all vehicles are equipped with GPS and V2X communication devices and the last vehicle is driven by a connected cruise controller. The blue arrows represent feedback terms using motion information received from multiple vehicles ahead. (b) Saturation function used in (7). (c,d) Switching functions (9) and (10) used to switch from connected car-following mode to cruising mode.

$$\dot{s}_0(t) = v_0(t),$$
$$\dot{v}_0(t) = \text{sat}\left(\sum_{i=1}^{n} u_i(t-\sigma_i)\right),$$

(7)

where u_i denotes the acceleration command in response to the motion of preceding vehicle i. The command signal is delayed by $\sigma_i = \xi_i + \zeta$ where ξ_i represents the delay of information from vehicle i due to sampling and communication intermittency. While ξ_i is stochastic and heterogeneous between different vehicles, we can assume $0.1 \leq \xi_i \leq 0.2$ [s] when the update rate is 10 [Hz] (Qin et al., 2017). Moreover, ζ is the actuator delay, which can be alternatively modelled by a first-order lag (Orosz, 2016; Zheng et al., 2016). In our experiments $\zeta \approx 0.5$ [s], though this value can be smaller, especially for electric vehicles. The function sat($\cdot$) is used to limit the overall acceleration command between $a_{\min} = -7$ [m/s²] and $a_{\max} = 3$ [m/s²]; see Fig. 3(b). While the actual acceleration may be further limited by the engine power, such limitations are not unique to the connected automated vehicle and thus are omitted as in

(1). Similarly, we omit effects such as air drag, rolling resistance and road grade in (7), since they can be compensated through lower-level controllers (Zhang et al., 2018).

Finally, the acceleration commands $u_1,...,u_n$ in (7) are

$$
\begin{aligned}
u_1 &= A(V_0(h_0)-v_0) + B_1(W(v_1)-v_0), \\
u_i &= B_i(W(v_i)-v_0),
\end{aligned}
\tag{8}
$$

for $i = 2,...,n$. Note that the acceleration commands $u_2,...,u_n$ only contain velocity feedback terms but not distance feedback terms. It is because the gains tend to be significantly smaller in the latter case in a multi-objective optimal design (Ge and Orosz, 2017). While headway, speed and acceleration feedback terms can appear in a general connected cruise control design (Ge and Orosz, 2014; Zhang and Orosz, 2016), we use the simplified version (8) in the first experimental demonstration of connected cruise control.

In (8), the feedback gains A and B_i can be varied when the distance between the connected automated vehicle and a preceding vehicle is beyond a certain threshold, that is,

$$
A(s_1,s_0) = \begin{cases} \alpha & \text{if} \quad (s_1-s_0-l_0) \leqslant h_{\text{sw},1}, \\ \alpha_{\text{cc}} & \text{if} \quad (s_1-s_0-l_0) > h_{\text{sw},1}, \end{cases}
\tag{9}
$$

and

$$
B_i(s_i,s_0) = \begin{cases} \beta_i & \text{if} \quad (s_i-s_0-l_0) \leqslant h_{\text{on},i}, \\ \beta_i \frac{s_i-s_0-l_0-h_{\text{sw},i}}{h_{\text{on},i}-h_{\text{sw},i}} & \text{if} \quad h_{\text{on},i} < (s_i-s_0-l_0) < h_{\text{sw},i}, \\ 0 & \text{if} \quad (s_i-s_0-l_0) \geqslant h_{\text{sw},i}, \end{cases}
\tag{10}
$$

for $i = 1,...,n$; see Fig. 3(c) and (d). Such switching mechanisms are introduced so that the connected automated vehicle does not consider speed information from vehicles too far ahead. We found that it is beneficial to align these switches with those in the range policy V_0 defined by (3), in particular, to use $h_{\text{on},i} \approx ih_{\text{go},0}$ and $h_{\text{sw},i} = h_{\text{on},i} + d$ where d describes the length of the intervals the gains are "switched on". Note that the longitudinal controller (7) and (8) changes from the connected car-following mode to the cruising mode when $(s_i-s_0-l_0) > h_{\text{sw},i}$. Similar switching strategies have been used in adaptive cruise controllers, where jerky transitions between car-following and cruising modes can be avoided with well-tuned parameters (Labuhn et al., 2003; Barber et al., 2009). The safety and performance guarantee of such controllers can be obtained through formal verification as shown in (Nilsson et al., 2017).

The parameters in the longitudinal controller (7) and (8) are chosen such that the connected automated vehicle is plant stable and head-to-tail string stable (Zhang and Orosz, 2016). Plant stability requires that when the preceding vehicles $1,...,n$ drive with the equilibrium speed v^* (5), the connected automated vehicle is able to converge to v^* regardless of its initial conditions. Since most human-driven vehicles are plant stable, it is not challenging for the connected automated vehicle to be plant stable (Orosz, 2016). On the other hand, head-to-tail string stability requires the connected automated vehicle to have less speed fluctuations compared with vehicle n, the farthest vehicle ahead whose motion information is used. Most human drivers are unable to suppress speed fluctuations propagating along the vehicle chain due to their large reaction time and the fact that they only monitor the motion of the vehicle immediately ahead (Orosz, 2016). Therefore, speed fluctuations for vehicle 1 are very likely to be more severe than for vehicle n. However, using motion information from vehicles farther ahead, the connected automated vehicle is able to regulate its speed fluctuations to be less than for vehicle n. In particular, feedback terms $u_2,...,u_n$ can create "additional phase lead" in the longitudinal controller (7) compared with using u_1 alone, which enables better speed regulation.

We note that making the connected cruise controller (7) and (8) head-to-tail string stable is a challenging task due to the rich behavior of the preceding human-driven vehicles. Here, we utilize the theoretical results in (Avedisov and Orosz, 2017; Zhang and Orosz, 2016; Qin and Orosz, 2017; Ge and Orosz, 2017; Zhang et al., 2018) to guide the parameter tuning in the controller proposed above. Although these publications claim theoretically that the controller is able to suppress the speed fluctuations under certain assumptions on human behaviors and V2X communication, the connected automated vehicle's performance needs to be tested against real human-driven vehicles and V2X communication devices, as we describe in the next section.

4. Experimental setup for connected automated vehicle design and evaluation

In this section we provide some technical details about the human-driven vehicles and the connected automated vehicle used in the experiments, and we introduce the experimental scenarios used for connected cruise control design and evaluation. All human-driven vehicles used in the experiments are production vehicles retrofitted with V2X devices that broadcast standard 10-Hz basic safety messages (BSM) under the dedicated short range communication (DSRC) protocol (FCC, 2016; SAE J2735, 2016). We remark however that the experiments may also be reproduced using different communication protocols (Festag, 2015). Each V2X device contains an electronic control unit (ECU) with antennae and can be powered through a 12 V auxiliary power outlet; see Fig. 4(b). In the experiments, human-driven vehicles only need to share their GPS position and speed data, which allows most production vehicles to be retrofitted in a plug-and-play style. As an example of such plug-and-play instrumentation, in Fig. 4(a) we show two human-driven vehicles (Nissan and Honda on the left and the middle) and the connected automated vehicle (Kia on the right) used in the experiments. The connected automated vehicle is capable of accelerating/decelerating and steering control by connecting the V2X device with a motion-control ECU and an upper-level computer for visualization.

We present three sets of experiments where the connected automated vehicle benefits from V2X communication. The first two sets

Fig. 4. (a) Two human-driven vehicles and one connected automated vehicle used in the experiments. The two vehicles on the left are only equipped with V2X communication devices, while the vehicle on the right is capable of automated driving as well as V2X communication. (b) The V2X communication device: 1 upper-level computer, 2 ethernet cable, 3 electronic control unit, 4 power cable, 5 GPS and V2X antennae.

of experiments are conducted in a testing facility where GPS map data are available. These experiments are reconstructions of safety-critical scenarios and demonstrate the benefits of adding V2X communication on the top of automation. The first set of experiments considers the scenario where the preceding vehicle is beyond the line of sight of a human driver due to road geometry and view obstruction. In similar scenarios, sensor-based driving automation may not be able to "see" the preceding vehicle until it gets to its vicinity requiring harsh braking to stop the vehicle. We demonstrate that V2X-based control can compensate for such perception failures and improve performance.

The second set of experiments considers the scenario where a sequence of harsh braking develops along a string of human-driven vehicles. In similar scenarios, an automated vehicle without V2X communication typically responds with the sudden harsh braking to keep a safe distance. We demonstrate that motion information from vehicles farther ahead can help the connected automated vehicle to respond with additional "phase lead" and avoid such sudden speed changes. These two sets of experiments highlight that driving automation without V2X communication is likely to enter safety-critical situations where sudden maneuvers are needed to keep a safe distance from the other vehicles. Such maneuvers however, apart from compromising passenger comfort, may not be possible to execute under less than ideal road conditions (e.g., reduced road friction). V2X-based control allows the connected automated vehicle to avoid entering such safety-critical situations.

The third set of experiments validates the benefits of connected cruise control following a chain of human-driven cars on public roads. In particular, we observe how speed fluctuations propagate along a chain of human-driven vehicles in front of the connected automated vehicle and demonstrate that, by using information from multiple preceding human-driven vehicles, the connected automated vehicle is able to mitigate these traffic waves. We quantify these benefits by showing that CCC reduces velocity and acceleration fluctuations and improves the energy efficiency of the connected automated vehicle and also the following human-driven vehicles. These experiments emphasize the benefits of V2X-based control for driving automation without the support of an automated platoon. In fact, we show that benefits can also be gained even in scenarios where not all human-driven vehicles are equipped with V2X devices so the connected automated vehicle is not aware of the presence of some of these vehicles.

5. Avoiding safety–critical scenarios on a closed track

To demonstrate the capabilities of the connected cruise controller (7) and (8) we use a closed track to reconstruct two scenarios that could push human-driven or automated vehicles without connectivity to the physical limits. We show that by using V2X information appropriately the connected automated vehicle can avoid the safety-critical states. The control parameters chosen through these experiments will also be utilized for tests carried out on public roads described in the next section.

5.1. A connected automated vehicle stopping behind a stationary vehicle on curvy road

Here we consider a scenario where a connected automated vehicle travels on a road with a right turn, as shown by the blue dashed
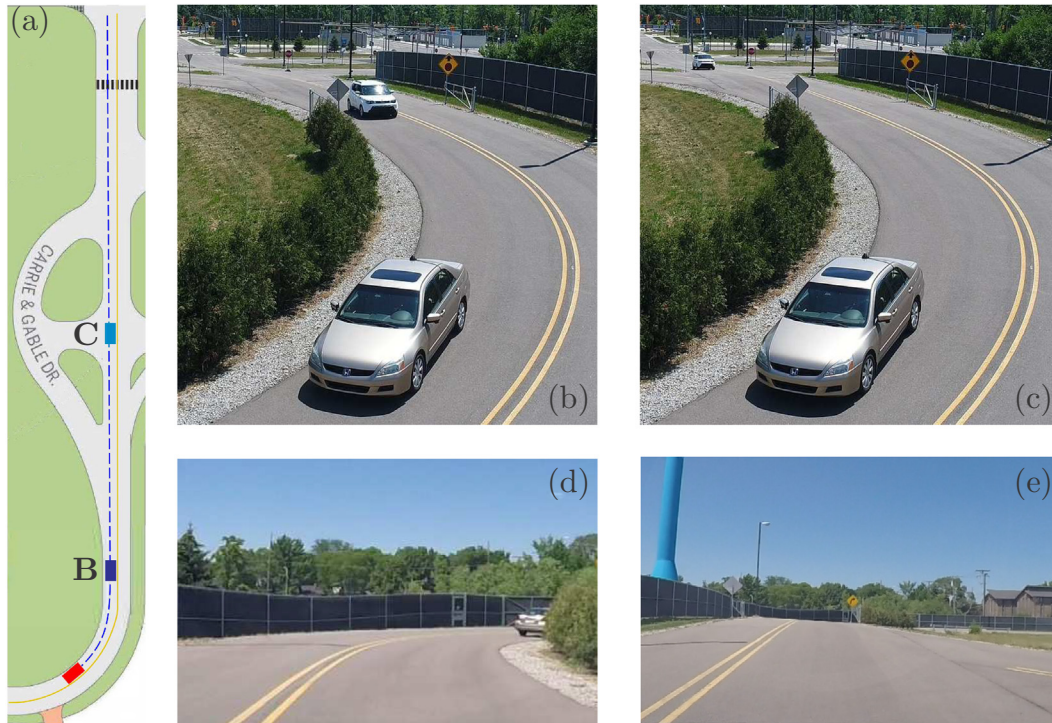
Fig. 5. Testing scenario for beyond-line-of-sight safety due to road geometry. (a) The road geometry with the red rectangle denoting a stationary vehicle. The dark blue rectangle denotes the human-driven vehicle at the location B where it starts to respond to the stationary vehicle, while the light blue rectangle denotes the connected automated vehicle at the location C where it starts to respond to the stationary vehicle. (b) Bird's eye view when the car is at position B. (c) Bird's eye view when the car is at position C. (d) Driver's view when the car is at position B. (e) Driver's view when the car is at position C. (For interpretation of the references to colour in this figure legend, the reader is referred to the web version of this article.)

trajectory in Fig. 5(a). Another vehicle is stopped where the road starts to turn, as marked by the red rectangle. Due to road curvature and elevation, a human driver or sensors would only be able to perceive the stationary vehicle shortly before entering the curve, as indicated by the dark blue rectangle at position B. At this moment, the distance between two the vehicles (dark blue and red) is about 25 meters. The corresponding bird's eye view is shown in Fig. 5(b) while the corresponding driver's view is shown in Fig. 5(d). Due to this sudden appearance of the stationary vehicle, a harsh braking must be applied to avoid collision.

Fig. 6(a) and (b) show the speed and acceleration profiles of a human-driven vehicle when it approaches this curve and responds to the stationary vehicle. At the beginning the driver accelerates the vehicle until it reaches a speed close to the speed limit (35 [mph] $\approx$ 15.6 [m/s]) and then tries to keep the speed constant. At around 20 [s], the driver sees the stationary vehicle, and a harsh braking follows. While the human driver is able to stop the vehicle safely, the deceleration reaches -8 [m/s^2]. Such deceleration may not always be achievable when the road surface is not ideal, and it may trigger a cascade of harsh braking among the following vehicles. In the same way, an automated vehicle that relies solely on sensors would also enter such hazardous situations due to obstructions of its line of sight.

To solve such a problem, we replace the human driver with the controller (7) and (8), where $n = 1$ since there is only one car ahead. For the range policy function $V_0(h_0)$, we set the distances $h_{st,0} = 5$ [m], $h_{go,0} = 30$ [m], and the speed limit $v_{max} = 15$ [m/s], such that the gradient becomes $\kappa_0 = 0.6$ [1/s]. The feedback gains are $\alpha_{cc} = 0.9$ [1/s], $\alpha = 0.2$ [1/s], $\beta_1 = 0.4$ [1/s], with switching distances $h_{on,1} = h_{go,0} = 30$ [m] and $h_{sw} = 70$ [m]. The speed and acceleration profiles of the connected automated vehicle are shown in Fig. 6(c) and (d). In Fig. 6(d), the thin green curve is the commanded acceleration, while the thick blue curve is the measured acceleration that the connected automated vehicle achieves. We note that the commanded acceleration cannot always be reached due to the limited engine power.

We observe that the measured speed and acceleration (thick curves) in Fig. 6(c) and (d) are fairly similar to the ones in Fig. 6(a) and (b) when $t < 10$ [s]. That is, the connected automated vehicle accelerates to the desired speed in a similar manner as a human-driven vehicle when the preceding vehicle is far away. However, as V2X communication informs the connected automated vehicle about the stationary vehicle behind the curve, it starts braking earlier, at position C marked by the light blue rectangle in Fig. 5(a) with the corresponding the bird's eye view and driver's view shown in Fig. 5(c) and (e). Correspondingly, the connected automated vehicle slows down in a much milder way: its deceleration only reaches -2 [m/s^2] in Fig. 6(d), which would remain safe with less than ideal road surfaces and is unlikely to trigger a cascade of harsh braking.

In Fig. 6(e) and (f) we show the speed and acceleration of both the human-driven vehicle (dark blue curves) and the connected automated vehicle (light blue curves) as function of position as the vehicle travels along the road. The stationary vehicle is located at
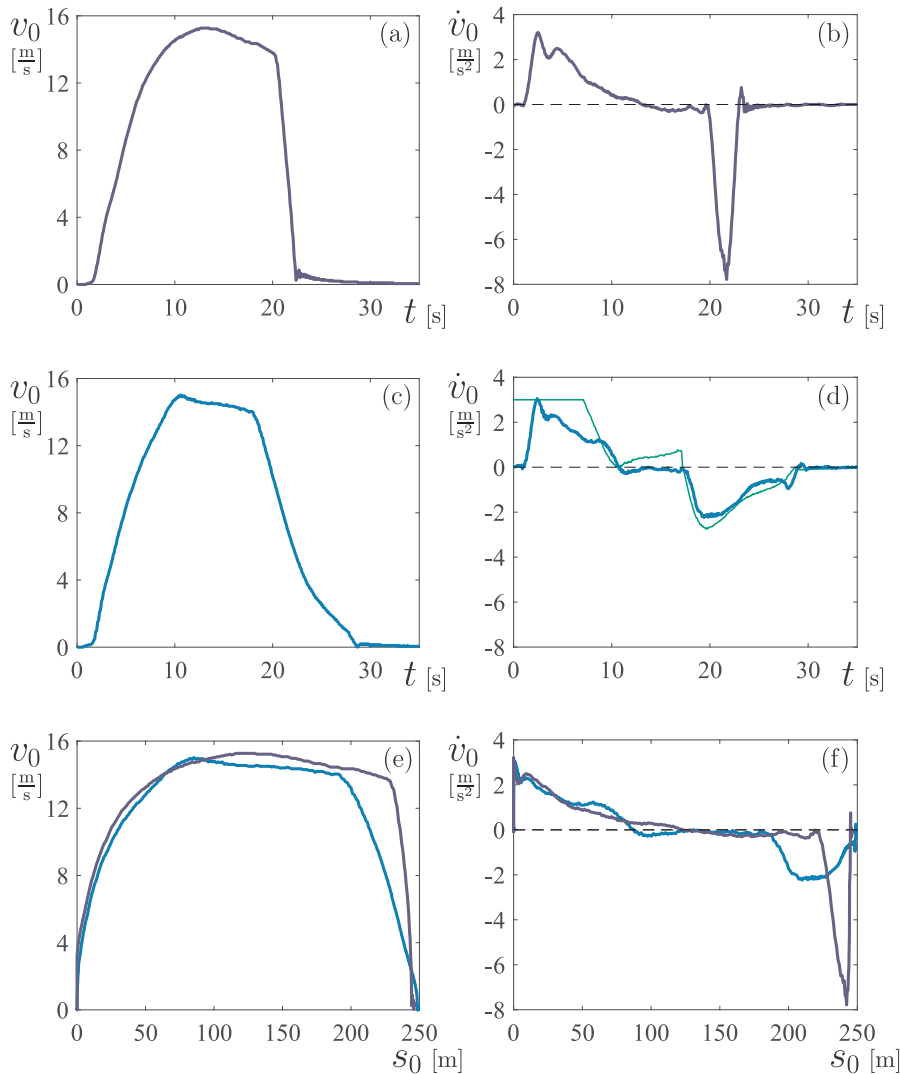
Fig. 6. Comparison of the human-driven vehicle (dark blue curves) and connected automated vehicle (light blue curves) approaching the stationary vehicle. (a,b) Speed and acceleration profiles of a human-driven vehicle as function of time. (c,d) Speed and acceleration profiles of a connected automated vehicle as function of time. In panel (d), the thin green curve shows the commanded acceleration from (7) and (8). (e) Speed as function of the position. (f) Acceleration as a function of the position. (For interpretation of the references to colour in this figure legend, the reader is referred to the web version of this article.)

$s_1 \equiv 260$ [m], while vehicle 0 travels from $s_0 = 0$ [m] to $s_0 \approx 250$ [m] in both cases, i.e., the distance headway h_0 varies between 5 [m] and 255 [m] when $l_0 = 5$ [m]. In Fig. 6(e) one may observe that in both cases the vehicle travels with similar speed before braking. Yet the human-driven vehicle only starts to brake at $s_0 \approx 230$ [m], i.e., when it is 25 meters from the stationary vehicle and the stationary vehicle becomes visible to the driver (see Fig. 5(b) and (d)). On the other hand, the connected automated vehicle starts to brake at $s_0 \approx 185$ [m], i.e., when it is $h_{sw,1} = 70$ meters from the stationary vehicle and the stationary vehicle is still beyond its line of sight (see Fig. 5(c) and (e)). As a result, the connected automated vehicle is able to avoid the harsh braking and the potential safety hazard, as shown in Fig. 6(f).

5.2. A connected automated vehicle handling a cascade of braking

Here we consider a scenario where a connected automated vehicle travels on a straight road behind three human-driven vehicles as shown in Fig. 7. We consider the traffic situation where the head vehicle (Nissan) decelerates and triggers a cascade of severe decelerations among the two following human-driven vehicles (Hondas). Such a phenomenon is quite common when human drivers are not sufficiently attentive to the changes in traffic. It is desirable that the connected automated vehicle does not only stay safe when driving behind human-operated cars, but also mitigate disturbances propagating from those. For the sake of clarity, cars are indicated as green, black, red, and blue in the following figures; see Fig. 8(a), and time profiles of speed, acceleration and distance

Fig. 7. A connected automated vehicle responding to a cascade of braking of human-driven vehicles.
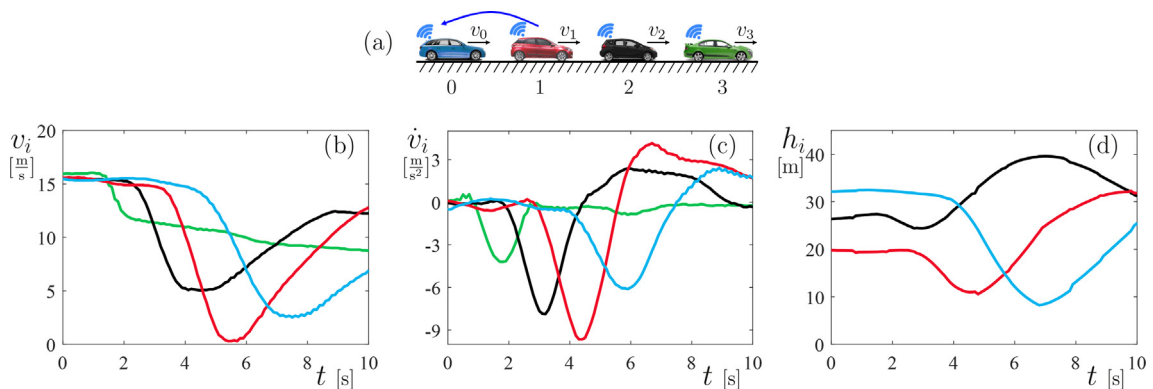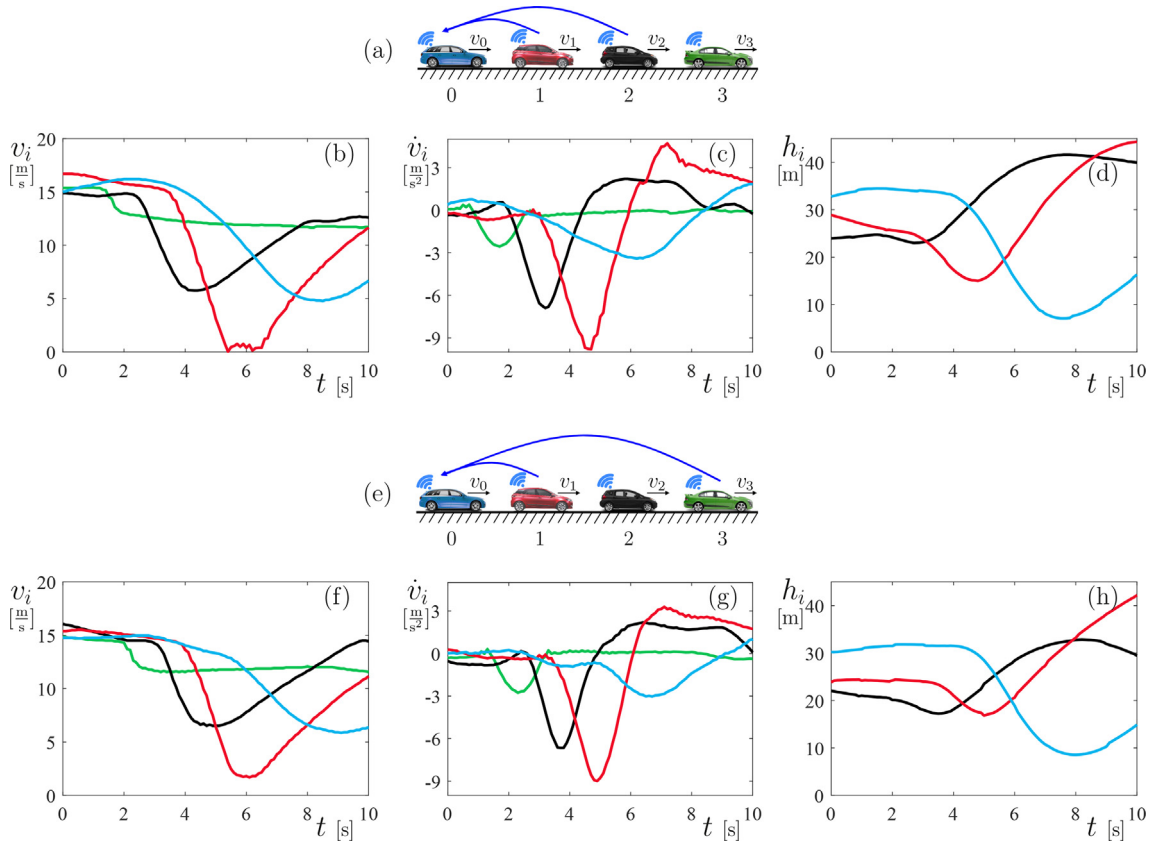

Fig. 8. A connected automated vehicle travels on a straight road behind three human-driven vehicles. (a) The connected automated vehicle only utilizes motion information from vehicle 1 with feedback gains $\alpha = 0.4$ [1/s], $\beta_1 = 0.5$ [1/s]. (b,c,d) Speed, acceleration, and distance headway profiles of the four vehicles during one experiment.

headway are depicted with the corresponding color as in Fig. 8(b)–(d). Notice that in Fig. 8(c), the deceleration rates of green, black, and red cars reach $-4, -8$, and -10 [m/s^2], respectively. That is, while the head vehicle 3 (green) brakes moderately, vehicle 1 (red) brakes at its physical limit while trying to keep its distance to the preceding vehicle.

To establish a baseline scenario we first consider the connected automated vehicle 0 (blue) only uses motion information from its immediate predecessor, vehicle 1 (red); as shown by the arrow in Fig. 8(a). Thus, we have $n = 1$ in (7), and we may say that this connected automated vehicle is "degraded" to an automated vehicle as it is not using beyond-line-of-sight information. For the range policy function $V_0(h_0)$, we set the distances $h_{st,0} = 5$ [m], $h_{go,0} = 35$ [m], and the speed limit $v_{max} = 18$ [m/s], so that the gradient remains $\kappa_0 = 0.6$ [1/s]. The feedback gains are selected as $\alpha = 0.4$ [1/s], $\beta_1 = 0.5$ [1/s] in order to ensure small steady state error in the distance headway when the vehicle immediately ahead is moving with constant speed as well as to ensure attenuation of perturbations imposed by the vehicle immediately ahead at all frequencies (string stability) despite having delay $\sigma_1 \leq 0.7$ in (7); see (Zhang and Orosz, 2016). The response of this connected automated vehicle with no beyond-line-of-sight information is plotted as blue curves in Fig. 8(b)–(d). We note that while it brakes milder than its immediate predecessor, its deceleration reaches -6 [m/s^2] and its speed is reduced significantly. While this vehicle might perform slightly better with more gain-tuning, without information from cars farther ahead the improvement to its performance will be limited.

To demonstrate the benefits of connected cruise control utilizing beyond-line-of-sight information, we then consider the cases where motion information from multiple vehicles ahead is available to the connected automated vehicle through V2X communication. We start with adding motion information from vehicle 2 (black), see Fig. 9(a). The corresponding gains are $\alpha = 0.4$ [1/s], $\beta_1 = 0.2$ [1/s], $\beta_2 = 0.3$ [1/s], which are again selected to ensure small steady state error and attenuation of perturbations coming from the vehicles ahead. Parameters in the range policy function are the same as in Fig. 8. In Fig. 9(b)–(d), the human-driven cars (green, black, and red curves) have similar motion profiles as in Fig. 8(b)–(d). In the mean time the connected automated car (blue) applies less severe braking with smaller speed oscillations and peak deceleration rate at -3.5 [m/s^2], without significantly reducing the minimum headway distance during the maneuver.

While (Zhang and Orosz, 2017) proposed an algorithm to identify which vehicle ahead a certain motion signal originates from, it can be challenging to pinpoint the exact number of cars between a transmitting vehicle and the connected automated vehicle at any time. Thus, we consider the case where signals from vehicle 3 (green) is used instead of vehicle 2 (black); see Fig. 9(e). The
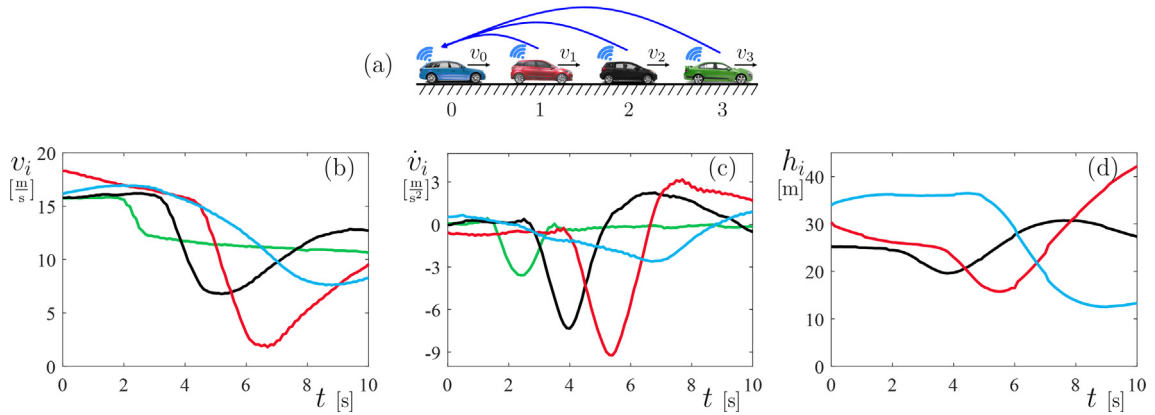
Fig. 9. A connected automated vehicle travels on a straight road behind three human-driven vehicles. (a) The connected automated vehicle utilizes motion information from vehicle 1 and vehicle 2 with feedback gains $\alpha = 0.4$ [1/s], $\beta_1 = 0.2$ [1/s], $\beta_2 = 0.3$ [1/s]. (b,c,d) Speed, acceleration, and distance headway profiles of the four vehicles during one experiment. (e) The connected automated vehicle utilizes motion information from vehicle 1 and vehicle 3 with feedback gains $\alpha = 0.4$ [1/s], $\beta_1 = 0.2$ [1/s], $\beta_3 = 0.3$ [1/s]. (f,g,h) Speed, acceleration, and distance headway profiles of the four vehicles during one experiment.

corresponding gains are $\alpha = 0.4$ [1/s], $\beta_1 = 0.2$ [1/s], $\beta_3 = 0.3$ [1/s], that is, exactly the same controller is used as in the previous case but with different connectivity topology. In Fig. 9(f)–(h) the connected automated vehicle 0 (blue) maintains a similar level of deceleration and similar distance as in Fig. 9(b)–(d), which demonstrates the robustness of connected cruise controller to changes in connectivity topology. The two cases in Fig. 9 demonstrate that using motion information from more than one vehicle ahead enables the connected automated vehicle to avoid severe braking maneuvers even when the vehicle immediately ahead deploys maximum braking. Moreover such performance is robust against uncertainties in the source of V2X information.

To further explore the potential of beyond-line-of-sight information, we consider the case where motion information from all three preceding vehicles is available; see Fig. 10(a). We use the same parameters as in Figs. 8 and 9, and the feedback gains are $\alpha = 0.4$ [1/s], $\beta_1 = 0.2$ [1/s], $\beta_2 = 0.3$ [1/s], $\beta_3 = 0.3$ [1/s] which are selected to ensure that the connected automated vehicle attenuates perturbations compared to the head vehicle 3 (that is, head-to-tail string stability is achieved). Corresponding to this in Fig. 10(c) the deceleration of the connected automated vehicle 0 (blue) peaks at -2.5 [m/s^2], compared with -6 [m/s^2] in Fig. 8(c) and -3.5 [m/s^2] in Fig. 9(c) and (g) while it actually maintains a slightly larger distance headway; cf. Fig. 10(d) with Fig. 9(d) and (h). Observe that the peak deceleration for the head vehicle 3 (green) is about -3.5 [m/s^2]. That is, the connected automated vehicle utilizing motion information from three preceding vehicles not only stays safe, but also stops the cascading of braking events. This illustrates how beyond-line-of-sight information can significantly improve active safety while also mitigating traffic waves.

6. Mitigating traffic waves on a public road

Based on the design established in the previous section, here we evaluate the performance of the controller (7) and (8) in real-world scenarios where the connected automated vehicle is traveling on a straight road behind six human-driven vehicles and followed by another human-driven vehicle. The vehicle at the front leads the vehicle chain with a series of mild braking events, a profile chosen because such mild speed perturbations have been observed frequently in urban and highway traffic. Through a series of experiments, we demonstrate that while motion perturbations are amplified as cascading backward along the chain of human-driven vehicles, the connected automated vehicle is able to mitigate such perturbations by using beyond-line-of-sight information. An

Fig. 10. A connected automated vehicle travels on a straight road behind three human-driven vehicles. (a) The connected automated vehicle utilizes motion information from all three preceding vehicle with feedback gains $\alpha = 0.4$ [1/s], $\beta_1 = 0.2$ [1/s], $\beta_2 = 0.3$ [1/s], $\beta_3 = 0.3$ [1/s]. (b,c,d) Speed, acceleration, and distance headway profiles of the four vehicles during one experiment.

illustration of a traffic wave triggered by a mild braking is depicted in Fig. 11(a). The higher density in the middle corresponds to lower speed of the vehicles. The experiments are carried out on an 8-mile long segment of single-lane public road highlighted as blue in Fig. 11(b). The set of controllers used in this section is essentially the same as in the previous section except the speed limit is increased to match that of the road.

6.1. Using motion information from one preceding vehicle

Again the vehicles are color coded as (brown, purple, orange, green, black, red, blue, pink) as shown in Fig. 12(a) where vehicle 0 (blue) still denotes the connected automated vehicle. Vehicle 6 (brown) maintains the average speed is about 20 [m/s] that is intercepted by mild braking events as shown in Fig. 12(b). In Fig. 12(c), we demonstrate how an automated vehicle with no beyond-line-of-sight information behaves during one mild braking event. (We remark that the responses to the other braking events look qualitatively similar despite the variations in the behavior of the human drivers ahead.) The controller (7) and (8) is implemented on vehicle 0 with $n = 1$ and feedback gains $\alpha = 0.4$ [1/s], $\beta_1 = 0.5$ [1/s], cf. Fig. 8(a). The range policy function has $h_{st,0} = 5$ [m], $h_{go,0} = 55$ [m], and the speed limit $v_{max} = 30$ [m/s], still yielding $\kappa_0 = 0.6$ [1/s].

In Fig. 12(c), vehicle 6 (brown) reaches minimum speed $v_6(t) \approx 14$ [m/s] at $t \approx 385$ [s]. As the braking event cascades along the vehicle chain, the minimum speed of vehicle 1 (red) immediately in front of the automated vehicle becomes $v_1(t) \approx 9$ [m/s] at $t \approx 391$ [s]. Using only motion information from vehicle 1, the minimum speed of the automated vehicle 0 reaches $v_0(t) \approx 10$ [m/s] at $t \approx 393$ [s], forcing the human-driven vehicle −1 behind (pink) to slow down to a similar speed value. As the minimum speed drops lower and lower along the vehicle chain, a stop-and-go traffic jam is highly likely to emerge, which typically leads to decreased traffic throughput (Orosz et al., 2010). Speed profiles in Fig. 12(c) demonstrate that an automated vehicle with no beyond-line-of-sight information has limited capability to mitigate cascading braking events.

To further discuss the performance without beyond-line-of-sight information, we consider the acceleration of each vehicle throughout the whole experiment shown in Fig. 12(b), and plot the histograms of the acceleration data in Fig. 12(d)–(k). From
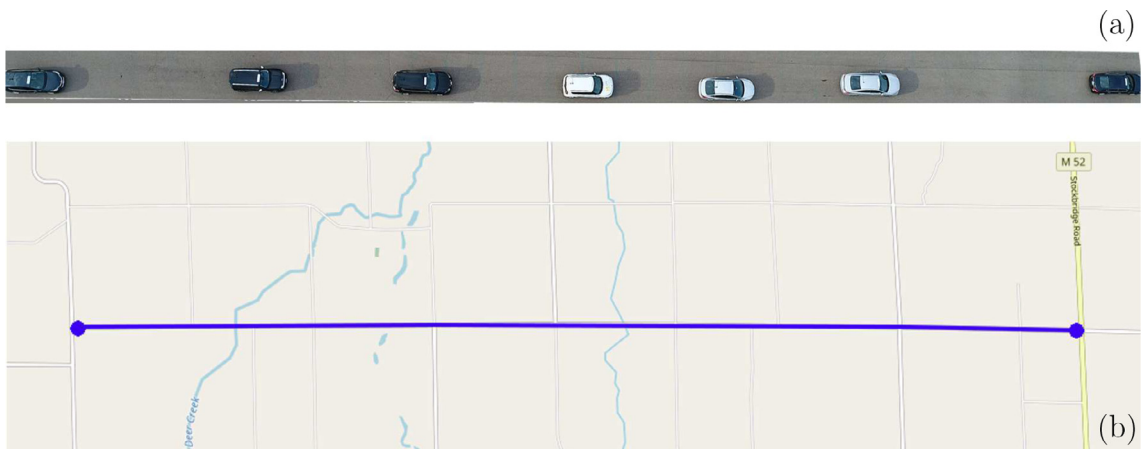

Fig. 11. (a) A traffic wave traveling on a group of connected vehicles. (b) The segment of road used for the experiments.
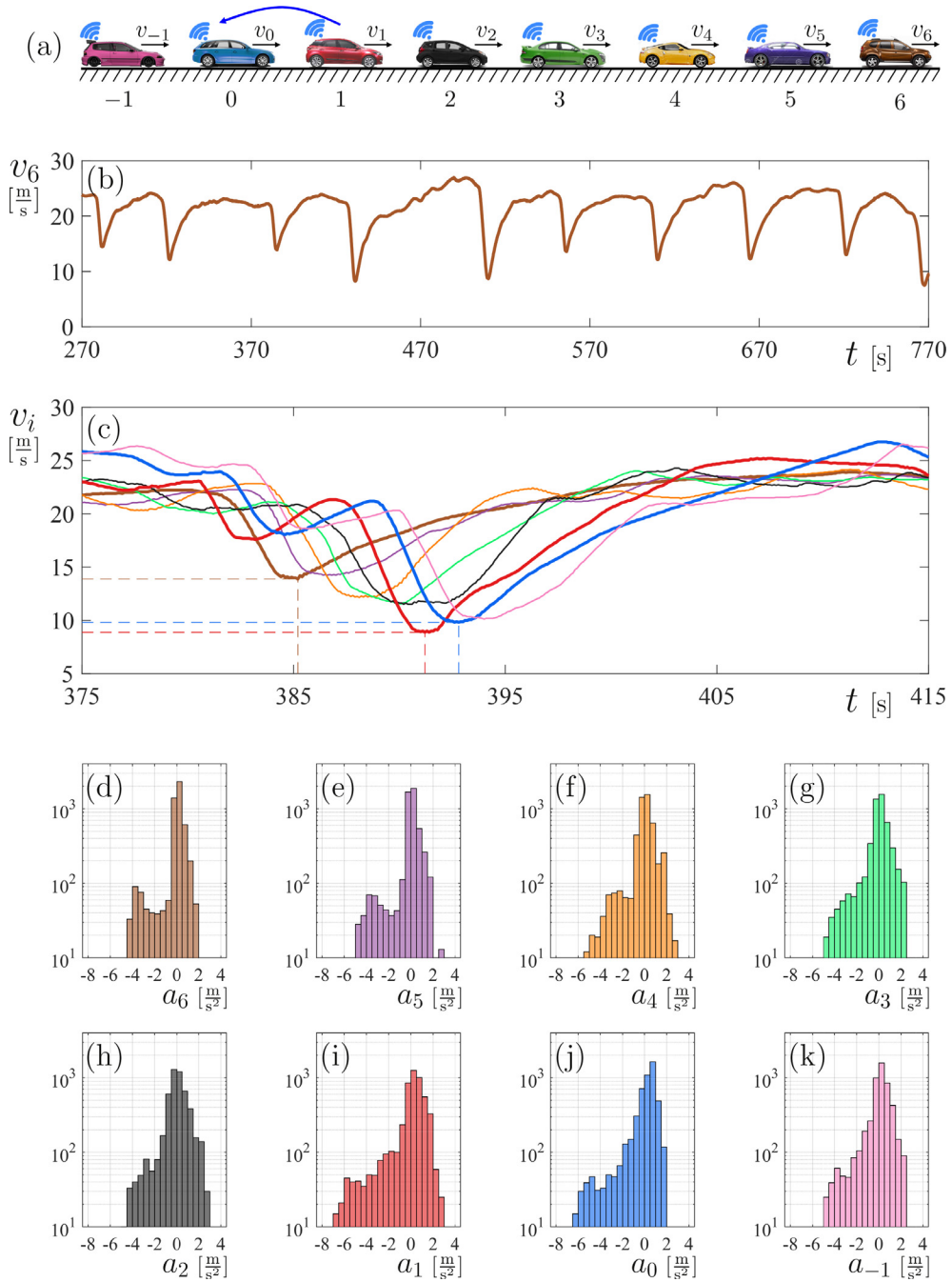
Fig. 12. (a) A connected automated vehicle (blue) traveling behind six human-driven vehicles while being followed by a human-driven vehicle (pink). The connected automated vehicle only utilizes motion information from vehicle 1 with feedback gains $\alpha = 0.4$ [1/s] and $\beta_1 = 0.5$ [1/s]. (b) The speed profile of vehicle 6. (c) Speed profiles of the eight vehicles during one braking event. (d-k) Histograms for the acceleration of the vehicles. (For interpretation of the references to colour in this figure legend, the reader is referred to the web version of this article.)

Fig. 12(d), we see that the range of the head vehicle's acceleration is $-5 \le a_6 \le 2$ [m/s²]. As the perturbations propagate, this range becomes $-7 \le a_2 \le 3$ [m/s²] for the car immediately in front of the automated vehicle, and the number of occurrences for acceleration above 2 [m/s²] and below -4 [m/s²] increases significantly; see Fig. 12(i). While Fig. 12(j) shows slightly fewer instances of severe braking and accelerating in the automated vehicle, the improvements are limited. The automated vehicle is also unable to induce significant improvements for the vehicle behind, as Fig. 12(k) shows many braking events around -6 [m/s²] (which could have raised safety hazards if the road conditions were less ideal).
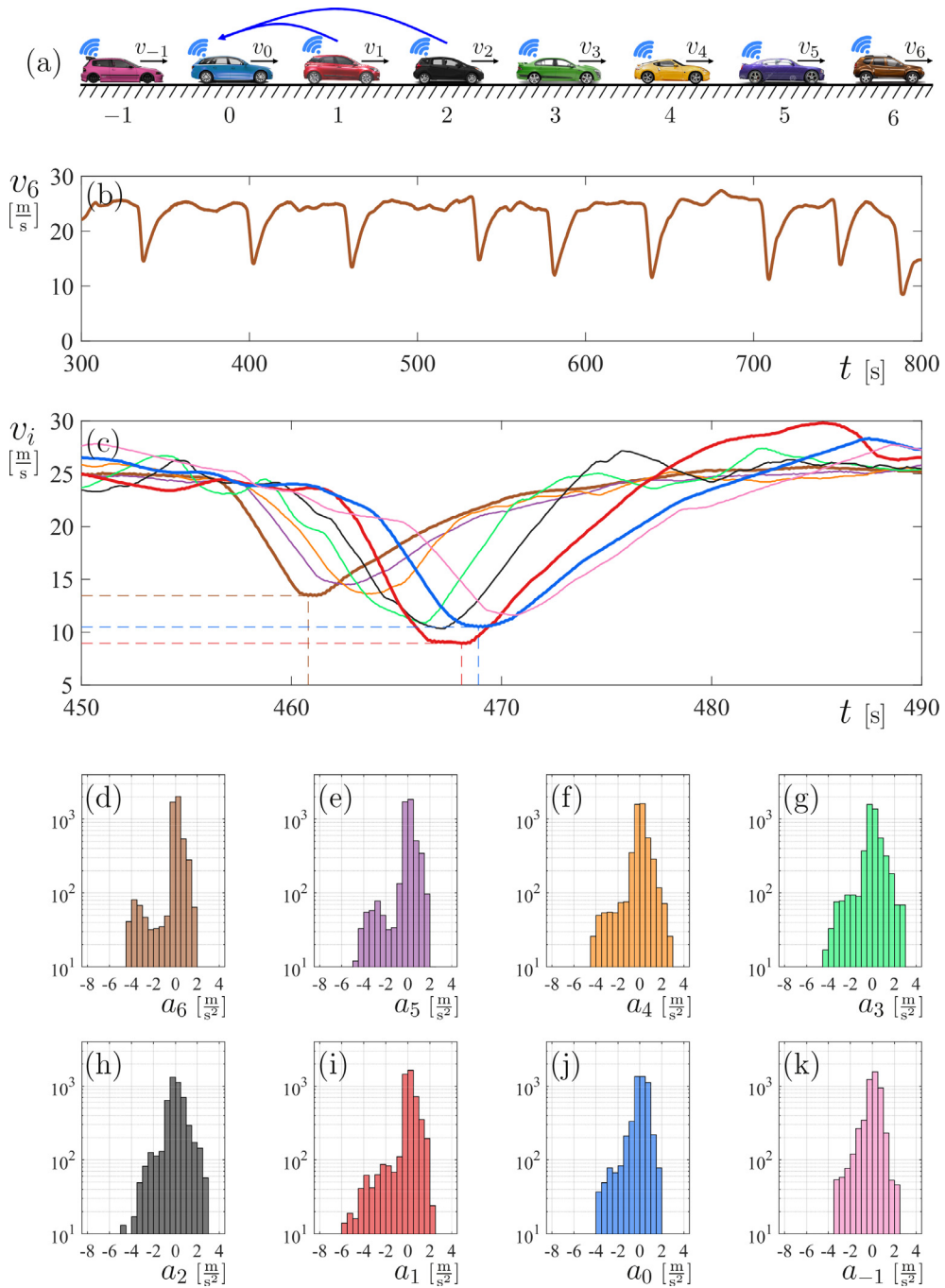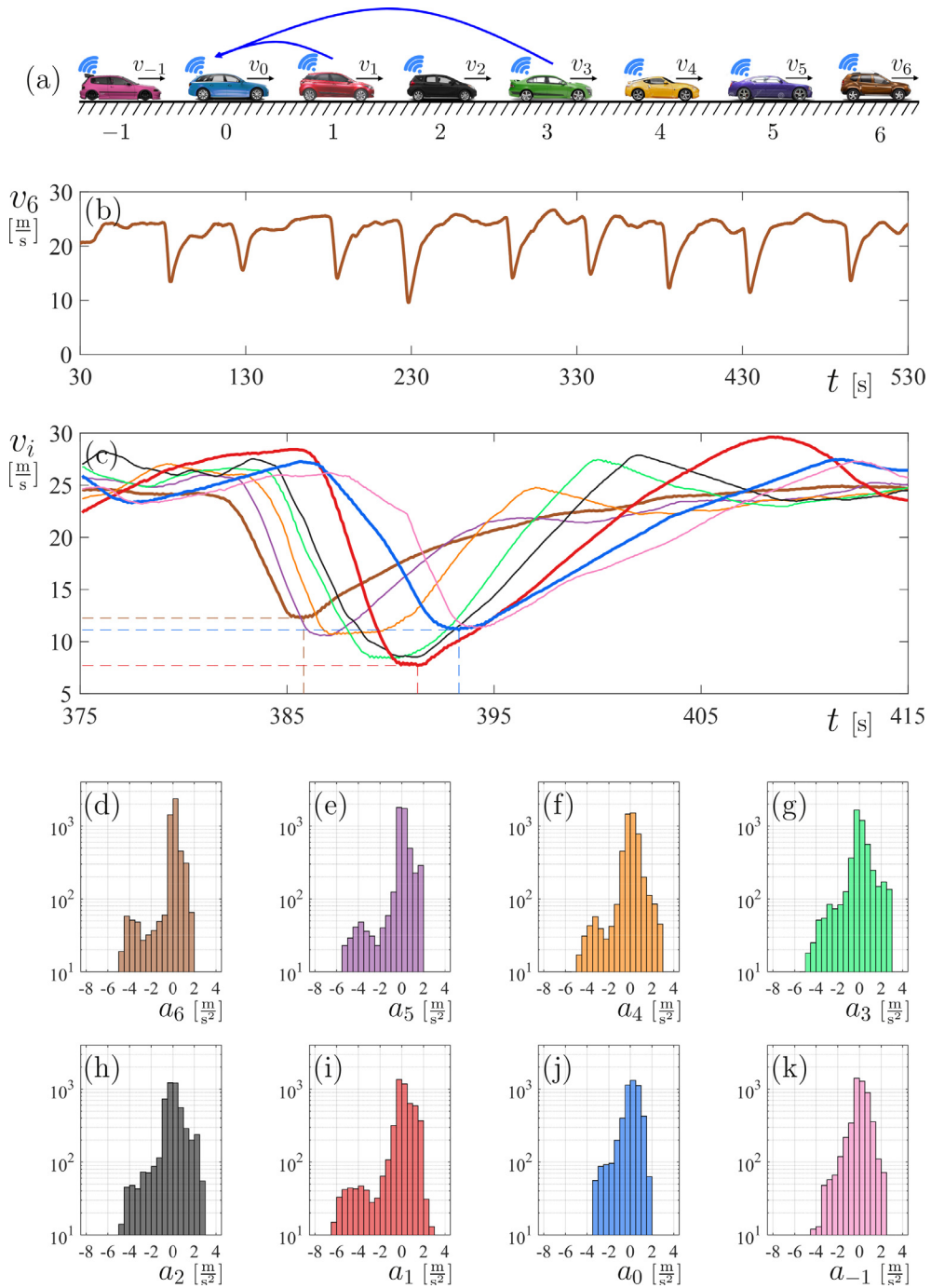
Fig. 13. (a) A connected automated vehicle (blue) traveling behind six human-driven vehicles while being followed by a human-driven vehicle (pink). The connected automated vehicle utilizes motion information from vehicle 1 and vehicle 2 with feedback gains $\alpha = 0.4$ [1/s], $\beta_1 = 0.2$ [1/s], and $\beta_2 = 0.3$ [1/s]. (b) The speed profile of vehicle 6. (c) Speed profiles of the eight vehicles during one braking event. (d-k) Histograms for the acceleration of the vehicles. (For interpretation of the references to colour in this figure legend, the reader is referred to the web version of this article.)

6.2. Using motion information from two preceding vehicles

Now we consider the cases where the connected automated vehicle uses motion information from two preceding vehicles. In Fig. 13(a) the blue car uses the connected cruise controller (7) and (8) with $n = 2$ and feedback gains $\alpha = 0.4$ [1/s], $\beta_1 = 0.2$ [1/s], and $\beta_2 = 0.3$ [1/s]; cf. Fig. 9(a). In Fig. 13(c) we still see the minimum speed decreasing from $v_6^{\min} \approx 14$ [m/s] to $v_1^{\min} \approx 9$ [m/s], while the connected automated vehicle brings its minimum speed above 10 [m/s]. Note that $\min\{v_0(t)\} \gtrsim \min\{v_2(t)\}$, that is, the adverse

Fig. 14. (a) A connected automated vehicle (blue) traveling behind six human-driven vehicles while being followed by a human-driven vehicle (pink). The connected automated vehicle utilizes motion information from vehicle 1 and vehicle 3 with feedback gains $\alpha = 0.4$ [1/s], $\beta_1 = 0.2$ [1/s], and $\beta_3 = 0.3$ [1/s]. (b) The speed profile of vehicle 6. (c) Speed profiles of the eight vehicles during one braking event. (d-k) Histograms for the acceleration of the vehicles. (For interpretation of the references to colour in this figure legend, the reader is referred to the web version of this article.)

influence of the human-driven vehicle 1 is successfully mitigated by the connected automated vehicle. Similar conclusions can be drawn from the acceleration histograms shown in Fig. 13(d)–(k). The histogram for the connected automated vehicle 0 (panel (j)) shows fewer instances of large accelerations and decelerations when compared with the preceding vehicles (panels (d)–(i)). As a result, vehicle −1, despite being human-driven, also exhibits motion with less harsh braking and acceleration; see panel (k). This illustrates the ability of the connected cruise controller (7) and (8) in mitigating traffic waves.

Similar as in Fig. 9(d), we consider the case where motion information from vehicle 3 is used instead of vehicle 2, that is, the feedback gains are $\alpha = 0.4$ [1/s], $\beta_1 = 0.2$ [1/s], and $\beta_3 = 0.3$ [1/s]; see Fig. 14(a). In Fig. 14(c), the connected automated vehicle again exhibits improvements in the speed cascading, as the minimum of v_0 is 3 [m/s] higher than the minimum of v_3. More importantly, when looking at the histograms in Fig. 14(d)–(k), we see fewer harsh braking/accelerating instances from the connected automated vehicle 0 (panel (j)) and the human-driven vehicle −1 (panel (k)) when compared with the preceding vehicles (panels (d)–(i)). This illustrates the robustness of the connected cruise controller (7) and (8) in mitigating traffic waves against uncertainties in the connectivity topology.

6.3. Using motion information from three preceding vehicles

Similar to Fig. 10(a), we consider the case when motion information from three preceding vehicles is used, that is, (7) and (8) with $n = 3$ and feedback gains $\alpha = 0.4$ [1/s], $\beta_1 = 0.2$ [1/s], $\beta_2 = 0.3$ [1/s], and $\beta_3 = 0.3$ [1/s]; see Fig. 15(a). In Fig. 15(c) we see larger minimum speed in the connected automated vehicle 0 and we clearly have $\min\{v_0(t)\} > \min\{v_3(t)\}$, which is related to the fact that the connected cruise controller is now robustly head-to-tail string stable. As a matter of fact, we have $\min\{v_0(t)\} \approx \min\{v_{-1}(t)\} > \min\{v_6(t)\}$ during the braking event shown here. In panels (d)-(i), we still see increasingly harsher acceleration/deceleration among human-driven cars. Yet panel (j) shows that the connected automated vehicle is able to maintain $a_0 \geq -3$ [m/s^2] except a few instances. As a result, the human-driven vehicle −1 behind also has milder braking than the lead vehicle 6; cf. panels (d) and (k). Thus, by using motion information from three preceding vehicles, the connected automated vehicle significantly mitigates the severe maneuvers from preceding vehicles so that even the following human-driven vehicle exhibits milder driving behavior than the lead vehicle. This indicates that we may start to see smoother traffic even when a low percentage of cars on road is appropriately using motion information from beyond their line of sight.

6.4. Improving energy efficiency with connected automated cars

Here we demonstrate benefits of using beyond-line-of-sight information on energy efficiency. In order to quantify this, we calculate the work per unit mass carried out by the power train of vehicle i during the time interval $[t_0,t]$ as

$$w_i(t) = \int_{t_0}^{t} g(\dot{v}_i(\theta) + f_i(v_i(\theta)))v_i(\theta)\mathrm{d}\theta, \tag{11}$$

for $i = -1,\ldots,6$. We refer to this as the energy consumption. Here we use $g(x) = \max(0,x)$ to select the cases when the engine carries out work and the energy dissipation due to rolling resistance and air drag are specified by $f_i(v_i) = a_i + c_i v_i^2$. While this may vary slightly for different vehicles here we use $a_i = 9.81 \cdot 10^{-2}$ [m/s^2], $c_i = 2.74 \cdot 10^{-4}$ [1/m] for all vehicles based on the characteristics of the connected automated vehicle. More detailed discussions on energy consumption may require high-fidelity powertrain model which is omitted here for simplicity (He and Orosz, 2017; He et al., 2018).

In Fig. 16 we show the energy consumption as functions of time for all the vehicles in the four experiments discussed earlier in this section while the numerical values at the end of the experiments are summarized in Fig. 16 (normed by the energy consumption of the least energy efficient vehicle in each experiment). Fig. 16(a) shows the energy consumption as a function of time when the automated vehicle is only using motion information from the car immediately ahead; see Fig. 12. Here, human-driven vehicles 6,…,1 consume increasingly more energy (brown, purple, orange, green, black, red curves), indicating that amplified traffic perturbations have adverse effects on energy efficiency. The automated vehicle (blue) consumes less energy than its immediate predecessor (red), but the difference is not significant.

Fig. 16(b) and (c) correspond to the two cases where motion information from two vehicles ahead is used; see Figs. 13 and 14, respectively. In both cases the connected automated vehicle (blue) consumes less energy than human-driven vehicles 1,2,3 (red, black, green), yet it still consumes more energy than human-driven vehicle 4 (orange). Fig. 16(d) corresponds to the case where the connected automated vehicle uses motion information from three preceding vehicles; see Fig. 15. In this case, the connected automated vehicle (blue) consumes less than vehicle 4 (orange) and only consumes 76% of the energy its immediate predecessor (red) at the end of the experiment. As a result, the human-driven vehicle behind (pink) only consumes 80% of the energy the red car uses. Table 1 also allows us to compare the energy consumption of vehicles in different experiments. In particular, when utilizing motion information from three preceding vehicles the connected automated vehicle 1 (blue) only consumes 81% of the energy compared to the case when it only uses information from its immediate predecessor. Calculating the same metric for the vehicle behind (pink), its energy consumption reduces to 93%. This shows that beyond-line-of-sight information may significantly improve the energy efficiency of connected automated vehicles and even human-driven vehicles following them.

7. Conclusion and discussion

In this paper, we proposed a general framework for the longitudinal control of connected automated vehicles and experimentally tested the performance of such connected cruise controllers that utilize beyond-line-of-sight information on real vehicles. We demonstrated that by using V2X communication, a connected automated vehicle is aware of a preceding vehicle obstructed by the road geometry, and is thus able to avoid a severe braking maneuver. We also demonstrated that by using motion information from multiple vehicles ahead, a connected automated vehicle is able to mitigate the cascade of braking events propagating from vehicles downstream. In both cases, the connected automated vehicle was able to keep a safe distance by applying mild braking in scenarios
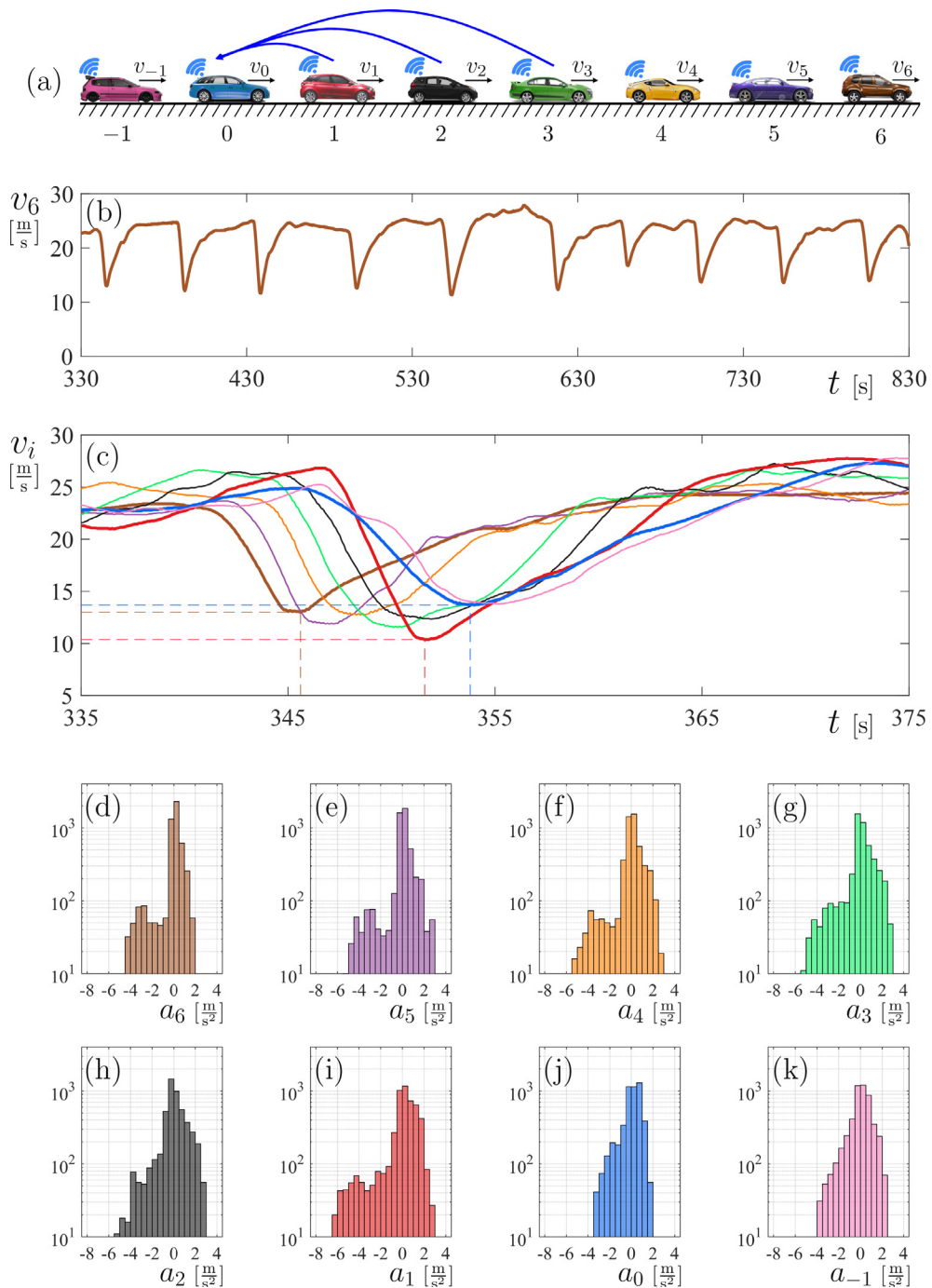
Fig. 15. (a) A connected automated vehicle (blue) traveling behind six human-driven vehicles while being followed by a human-driven vehicle (pink). The connected automated vehicle utilizes motion information from all three preceding vehicles with feedback gains $\alpha = 0.4$ [1/s], $\beta_1 = 0.2$ [1/s], $\beta_2 = 0.3$ [1/s], and $\beta_3 = 0.3$ [1/s]. (b) The speed profile of vehicle 6. (c) Speed profiles of the eight vehicles during one braking event. (d-k) Histograms for the acceleration of the vehicles. (For interpretation of the references to colour in this figure legend, the reader is referred to the web version of this article.)

where an automated vehicle had to apply harsh braking.

Then we evaluated our design through a set of eight-car experiments and showed that a connected automated vehicle using motion information from more than one vehicle ahead is able to mitigate traffic waves traveling along the chain of human-driven vehicles. This benefited not only the connected automated vehicle itself but also the human-driven vehicles following it. These benefits were quantified through the increase in minimum speed as well as the "narrowing" of acceleration distributions of the
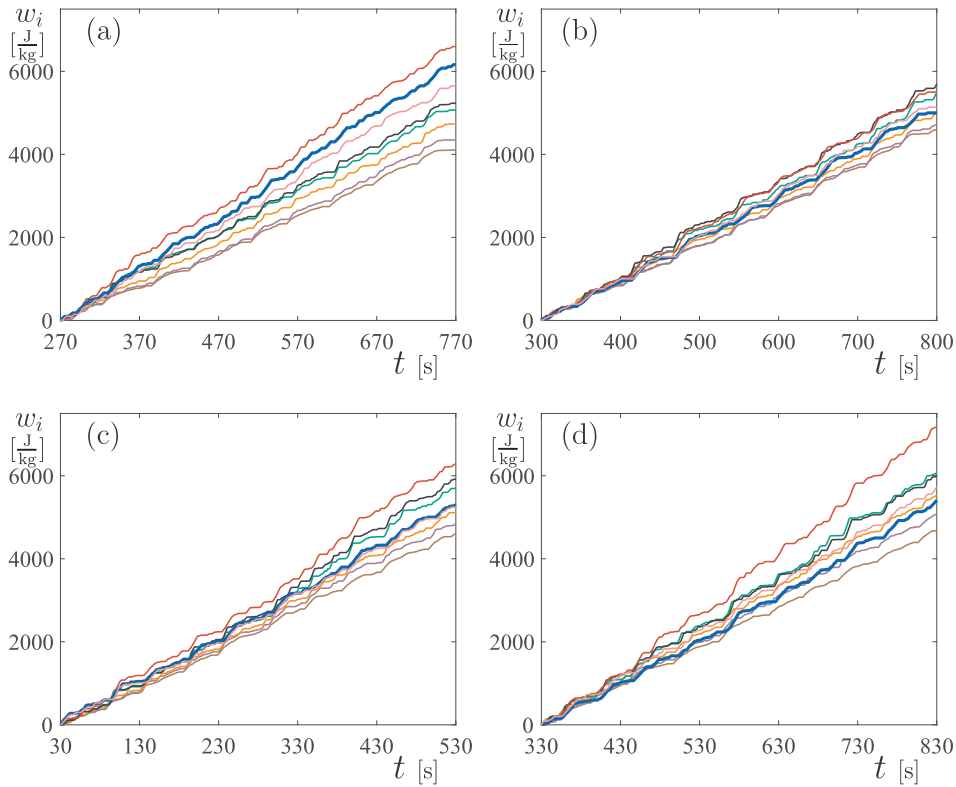
Fig. 16. Energy consumption of vehicles in four experiments. Panels (a–d) correspond to Figs. 12–15, respectively.

Table 1
The energy consumption at the end of the experiments shown in Fig. 16 normed by the energy consumption of the least energy efficient vehicle in each experiment.

	Fig. 16(a)	Fig. 16(b)	Fig. 16(c)	Fig. 16(d)
Car #6 (brown)	63	81	73	65
Car #5 (purple)	66	83	77	71
Car #4 (orange)	72	87	81	77
Car #3 (green)	77	96	91	85
Car #2 (black)	79	100	94	84
Car #1 (red)	100	97	100	100
Car #0 (blue)	93	88	84	76
Car #−1(pink)	86	90	83	80

connected automated vehicle and its followers while responding to traffic perturbations. Such improvements may positively influence safety in real-world scenarios. We also quantified the benefits in terms of energy efficiency, which may yield decreased fuel consumption for vehicles with internal combustion engine and increased range for electric vehicles.

The experiments presented in this paper suggest that connected cruise control can have a positive influence on traffic flow since by not allowing traffic waves to be fully formed it may prevent the formation of stop-and-go traffic jams that lead to decreased traffic throughput. However, more diverse scenarios need to be considered to demonstrate such improvement in multi-lane carriageways. In particular, lane changes play an important role in multi-lane traffic and connected automated vehicles may benefit from V2X information when executing such maneuvers. Investigating such scenarios theoretically and experimentally is left for future research.

Acknowledgment

References

Aeberhard, M., Rauch, S., Bahram, M., Tanzmeister, G., Thomas, J., Pilat, Y., Homm, F., Huber, W., Kaempchen, N., 2015. Experience, results and lessons learned from automated driving on Germany's highways. IEEE Intell. Transp. Syst. Mag. 7 (1), 42–57.

Avedisov, S.S., Orosz, G., 2017. Analysis of connected vehicle networks using network-based perturbation techniques. Nonlinear Dyn. 89 (3), 1651–1672.

Barber, P., Engelman, G., King, P., Richardson, M., 2009. Adaptive cruise control system and methodology, including control of inter-vehicle spacing. EP Patent 1,008,482.

California DMV, 2016. Autonomous Vehicle Disengagement Reports 2016. <https://www.dmv.ca.gov/portal/dmv/detail/vr/autonomous/disengagement_report_2016>.

di Bernardo, M., Salvi, A., Santini, S., 2015. Distributed consensus strategy for platooning of vehicles in the presence of time varying heterogeneous communication delays. IEEE Trans. Intell. Transp. Syst. 16 (1), 102–112.

Englund, C., Chen, L., Ploeg, J., Semsar-Kazerooni, E., Voronov, A., Bengtsson, H.H., Didoff, J., 2016. The grand cooperative driving challenge 2016: boosting the introduction of cooperative automated vehicles. IEEE Wirel. Commun. 23 (4), 146–152.

FCC, 2016. Dedicated Short Range Communications (DSRC) Service. <https://www.fcc.gov/dedicated-short-range-communications-dsrc-service>.

Festag, A., 2015. Standards for vehicular communication – from IEEE 802.11p to 5G. Elektrotechnik Informationstechnik 132 (7), 409–416.

Ge, J.I., Orosz, G., 2014. Dynamics of connected vehicle systems with delayed acceleration feedback. Transp. Res. Part C 46, 46–64.

Ge, J.I., Orosz, G., 2016. Estimation of feedback gains and delays in connected vehicle systems. In: Proceedings of the American Control Conference. IEEE, pp. 6000–6005.

Ge, J.I., Orosz, G., 2017. Optimal control of connected vehicle systems with communication delay and driver reaction time. IEEE Trans. Intell. Transp. Syst. 18 (8), 2056–2070.

Ge, J.I., Orosz, G., Hajdu, D., Insperger, T., Moehlis, J., 2017. To delay or not to delay – stability of connected cruise control. In: In: Orosz, G., Ersal, T., Insperger, T. (Eds.), Time Delay Systems – Theory, Numerics, Applications and Experiments. of Advances in Delays and Dynamics, vol. 7. Springer, pp. 263–282.

Harding, J., Powell, G., Yoon, R., Fikentscher, J., Doyle, C., Sade, D., Lukuc, M., Simons, J., Wang, J., 2014. Vehicle-to-vehicle communications: Readiness of V2V technology for application. Tech. Rep. DOT HS 812 014, National Highway Traffic Safety Administration.

He, C.R., Ge, J.I., Orosz, G., 2018. Data-based fuel-economy optimization of connected automated trucks in traffic. In: Proceedings of the American Control Conference. IEEE (in press).

He, C.R., Orosz, G., 2017. Saving fuel using wireless vehicle-to-vehicle communication. In: Proceedings of the American Control Conference. IEEE, pp. 4946–4951.

Jiang, H., Hu, J., An, S., Wang, M., Park, B.B., 2017. Eco approaching at an isolated signalized intersection under partially connected and automated vehicles environment. Transp. Res. Part C 79 (Supplement C), 290–307.

Labuhn, P.I., Chundrlik, W.J., Schmidt, E.H., 2003. Adaptive cruise control. US Patent 6,622,810 B2.

Li, S.E., Qin, X., Zheng, Y., Wang, J., Li, K., Zhang, H., 2017. Distributed platoon control under topologies with complex eigenvalues: stability analysis and controller synthesis. IEEE Trans. Control Syst. Technol.

Lioris, J., Pedarsani, R., Tascikaraoglu, F.Y., Varaiya, P., 2017. Platoons of connected vehicles can double throughput in urban roads. Transp. Res. Part C 77, 292–305.

Luo, Y., Xiang, Y., Cao, K., Li, K., 2016. A dynamic automated lane change maneuver based on vehicle-to-vehicle communication. Transp. Res. Part C 62, 87–102.

Mersky, A.C., Samaras, C., 2016. Fuel economy testing of autonomous vehicles. Transp. Res. Part C 65, 31–48.

Milanes, V., Alonso, J., Bouraoui, L., Ploeg, J., 2011. Cooperative maneuvering in close environments among cybercars and dual-mode cars. IEEE Trans. Intell. Transp. Syst. 12 (1), 15–24.

Milanes, V., Shladover, S.E., 2014. Modeling cooperative and autonomous adaptive cruise control dynamic responses using experimental data. Transp. Res. Part C 48, 285–300.

Montemerlo, M.S., Murveit, H.J., Urmson, C.P., Dolgov, D.A., Nemec, P., 2015. Determining when to drive autonomously. US Patent 8718861.

Nilsson, P., Hussien, O., Balkan, A., Chen, Y., Ames, A.D., Grizzle, J.W., Ozay, N., Peng, H., Tabuada, P., 2017. Correct-by-construction adaptive cruise control: two approaches. IEEE Trans. Control Syst. Technol. 24 (4), 1294–1307.

NTSHA, 2016. 2015 Motor Vehicle Crashes: Overview. Tech. rep., National Highway Traffic Safety Administration, <https://crashstats.nhtsa.dot.gov/Api/Public/ViewPublication/812318>.

Orosz, G., 2016. Connected cruise control: modeling, delay effects, and nonlinear behavior. Veh. Syst. Dyn. 54 (8), 1147–1176.

Orosz, G., Ge, J.I., He, C.R., Avedisov, S.S., Qin, W.B., Zhang, L., 2017. Seeing beyond the line of sight - controlling connected automated vehicles. ASME Mech. Eng. Mag. 139 (12), S8–S12.

Orosz, G., Wilson, R.E., Stépán, G., 2010. Traffic jams: dynamics and control. Philos. Trans. Roy. Soc. A 368 (1928), 4455–4479.

Ploeg, J., Shukla, D., van de Wouw, N., Nijmeijer, H., 2014a. Controller synthesis for string stability of vehicle platoons. IEEE Trans. Intell. Transp. Syst. 15 (2), 845–865.

Ploeg, J., van de Wouw, N., Nijmeijer, H., 2014b. $\mathscr{L}_p$ string stability of cascaded systems: application to vehicle platooning. IEEE Trans. Control Syst. Technol. 22 (2), 786–793.

Qin, W.B., Gomez, M.M., Orosz, G., 2017. Stability and frequency response under stochastic communication delays with applications to connected cruise control design. IEEE Trans. Intell. Transp. Syst. 18 (2), 388–403.

Qin, W.B., Orosz, G., 2017. Scalable stability analysis on large connected vehicle systems subject to stochastic communication delays. Transp. Res. Part C 83, 39–60.

SAE J2735, 2016. Dedicated Short Range Communications (DSRC) Message Set Dictionary Set. Tech. rep., SAE International.

Schrank, D., Eisele, B., Lomax, T., Bak, J., 2015. 2015 Annual Urban Mobility Scorecard. Progressreport, Texas Transportation Institute, College Station, TX.

Sepulcre, M., Gozalvez, J., Hernandez, J., 2013. Cooperative vehicle-to-vehicle active safety testing under challenging conditions. Transp. Res. Part C 26, 233–255.

Shladover, S., Su, D., Lu, X.-Y., 2012. Impacts of cooperative adaptive cruise control on freeway traffic flow. Transp. Res. Rec. 2324, 63–70.

Shladover, S.E., 2007. PATH at 20 - history and major milestones. IEEE Trans. Intell. Transp. Syst. 8 (4), 584–592.

Shladover, S.E., Nowakowski, C., Lu, X.-Y., Ferlis, R., 2015. Cooperative adaptive cruise control definitions and operating concepts. Transp. Res. Rec. 2489, 145–152.

Stern, R., Cui, S., Delle Monache, M.L., Bhadani, R., Bunting, M., Churchill, M., Hamilton, N., Haulcy, R., Pohlmann, H., Wu, F., Piccoli, B., Seibold, B., Sprinkle, J., Work, D., 2018. Dissipation of stop-and-go waves via control of autonomous vehicles: field experiments. Transp. Res. Part C 7 (1), 42–57.

Talebpour, A., Mahmassani, H.S., 2016. Influence of connected and autonomous vehicles on traffic flow stability and throughput. Transp. Res. Part C 71, 143–163.

Turri, V., Besselink, B., Johansson, K.H., 2017. Cooperative look-ahead control for fuel-efficient and safe heavy-duty vehicle platooning. IEEE Trans. Control Syst. Technol. 25 (1), 12–28.

Urmson, C.P., Dolgov, D.A., Chatham, A.H., Nemec, P., 2017. System and method of providing recommendations to users of vehicles. US Patent 9658620.

van Arem, B., van Driel, C.J.G., Visser, R., 2006. The impact of cooperative adaptive cruise control on traffic-flow characteristics. IEEE Trans. Intell. Transp. Syst. 7 (4), 429–436.

van Nunen, E., Kwakkernaat, R.J.A.E., Ploeg, J., Netten, B.D., 2012. Cooperative competition for future mobility. IEEE Trans. Intell. Transp. Syst. 13 (3), 1018–1025.

Vander Werf, J., Shladover, S., Miller, M., Kourjanskaia, N., 2002. Effects of adaptive cruise control systems on highway traffic flow capacity. Transp. Res. Rec. 1800, 78–84.

Wagner, P., 2010. Fluid-dynamical and microscopic description of traffic flow: a data-driven comparison. Philos. Trans. Roy. Soc. London A 368 (1928), 4481–4495.

Wang, M., Daamen, W., Hoogendoorn, S.P., van Arem, B., 2014a. Rolling horizon control framework for driver assistance systems. Part I: Mathematical formulation and non-cooperative systems. Transp. Res. Part C 40, 271–289.

Wang, M., Daamen, W., Hoogendoorn, S.P., van Arem, B., 2014b. Rolling horizon control framework for driver assistance systems. Part II: Cooperative sensing and cooperative control. Transp. Res. Part C 40, 290–311.

Zhang, L., Orosz, G., 2016. Motif-based analysis of connected vehicle systems: delay effects and stability. IEEE Trans. Control Syst. Technol. 17 (6), 1638–1651.

Zhang, L., Orosz, G., 2017. Beyond-line-of-sight identification by using vehicle-to-vehicle communication. IEEE Trans. Intell. Transp. Syst.

Zhang, L., Sun, J., Orosz, G., 2018. Hierarchical design of connected cruise control in the presence of information delays and uncertain vehicle dynamics. IEEE Trans. Control Syst. Technol. 26 (1), 139–150.

Zheng, Y., Li, S.E., Li, K., Borrelli, F., Hedrick, J.K., 2017. Distributed model predictive control for heterogeneous vehicle platoons under unidirectional topologies. IEEE Trans. Control Syst. Technol. 25 (3), 899–910.

Zheng, Y., Li, S.E., Wang, J., Cao, D., Li, K., 2016. Stability and scalability of homogeneous vehicular platoon: study on the influence of information flow topologies. IEEE Trans. Intell. Transp. Syst. 17 (1), 14–26.

Zhou, Y., Ahn, S., Chitturi, M., Noyce, D.A., 2017. Rolling horizon stochastic optimal control strategy for ACC and CACC under uncertainty. Transp. Res. Part C 83, 61–76.